An Improved Extreme Learning Machine (ELM) Algorithm for Intent Recognition of Transfemoral Amputees With Powered Knee Prosthesis

Yao Zhang, Xu Wang, Haohua Xiu, Wei Chen, Yongxin Ma, Guowu Wei, *Member, IEEE*, Lei Ren, *Member, IEEE*, and Luquan Ren

Abstract—To overcome the challenges posed by the complex structure and large parameter requirements of existing classification models, the authors propose an improved extreme learning machine (ELM) classifier for human locomotion intent recognition in this study, resulting in enhanced classification accuracy. The structure of the ELM algorithm is enhanced using the logistic regression (LR) algorithm, significantly reducing the number of hidden layer nodes. Hence, this algorithm can be adopted for real-time human locomotion intent recognition on portable devices with only 234 parameters to store. Additionally, a hybrid grey wolf optimization and slime mould algorithm (GWO-SMA) is proposed to optimize the hidden layer bias of the improved ELM classifier. Numerical results demonstrate that the proposed model successfully recognizes nine daily motion modes including low-, mid-, and fast-speed level ground walking, ramp ascent/descent, sit/stand, and stair ascent/descent. Specifically, it achieves 96.75% accuracy with 5-fold cross-validation while main- taining a real-time prediction time of only 2 ms. These promising findings highlight the potential of onboard real-time recognition of continuous locomotion modes based on our model for the high-level control of powered knee prostheses.

Index Terms—Extreme learning machine, human loco- motion intent recognition, real-time prediction, powered knee prosthesis.

Yao Zhang, Xu Wang, Wei Chen, Yongxin Ma, and Luquan Ren are with the Key Laboratory of Bionic Engineering, Ministry of Education, Jilin University, Changchun 130022, China (e-mail: yaoz20@mails.jlu.edu.cn; wx19@mails.jlu.edu.cn; chenwei_jlu@jlu. edu.cn; yongxin21@mails.jlu.edu.cn; lqren@jlu.edu.cn).

Haohua Xiu was with the Key Laboratory of Bionic Engineering, Min- istry of Education, Jilin University, Changchun 130022, China. He is now with the Robotics Institute of NBUT, Ningbo University of Technology, Ningbo 315211, China (e-mail: xiuhh@nbut.edu.cn).

Guowu Wei is with the School of Science, Engineering and Environment, University of Salford, M5 4WT Salford, U.K. (e-mail: g.wei@salford.ac.uk).

Lei Ren is with the Key Laboratory of Bionic Engineering, Ministry of Education, Jilin University, Changchun 130022, China, and also with the Department of Mechanical, Aerospace and Civil Engineering, The University of Manchester, M13 9PL Manchester, U.K. (e-mail: lren@jlu.edu.cn).

I. Introduction

LOWER limb amputation can cause difficulties in the daily locomotion of amputees, especially for transfemoral amputees. Thus, the utilization of a powered prosthesis capable of perceiving external environments and recognizing human locomotion intent could greatly improve the mobility of amputees [1], [2]. Although there are numerous machine learning algorithms that have been applied to human loco- motion intent recognition, some may not appropriate for real-time applications due to their complex structure and extensive parameter requirements that consume substantial memory space in embedded systems [3], [4]. On the other hand, the accuracy of the algorithm is extremely impor- tant as misclassifications can pose serious risks such as falls for amputees [5]. Previously proposed algorithms have demonstrated high accuracy in locomotion mode recogni- tion, including linear discriminant analysis (LDA) [6], hidden Markov model [7], support vector machine (SVM) [8], and quadratic discriminant analysis (QDA) [9]. Neural network algorithms have also been used for locomotion intent recog- nition in powered intelligent lower limb prostheses with promising classification accuracy rates [10], [11], [12]. How- ever, two challenges still impede the implementation of these algorithms in real-time detection of human locomotion inten- tions: preserving all parameters within complex networks, and the gradient-based learning methods used in neural network training are slow.

It is crucial to find an algorithm that exhibits fast learning speed and minimal training error. Huang et al. introduced the extreme learning machine (ELM) algorithm, which shares the same network structure as single hidden layer feedforward neural networks. However, unlike traditional approaches, ELM does not require tuning of hidden layer nodes; instead, the input weights are randomly generated and the output weights

are determined analytically [13]. By utilizing the output layer weights, the algorithm can compute network output and predict data effectively. Consequently, the proposed algorithm demonstrates exceptional generalization performance with extremely fast learning speed. Over the past few decades, Many improved versions of the ELM algorithm have been proposed including incremental ELM [14], pruned ELM [15], voting-based ELM [16], and ELM autoencoders [17]. The latest advancement in the evolution of ELM is the deep ELM (DELM) algorithm, which was proposed by Ding et al., where feature extraction and classification are treated as two separate parts without requiring parameter fine-tuning for the entire system. Thus, DELM achieves significantly faster training speed compared to traditional BPNN methods. Recently, several improved DELM algorithms have emerged with a focus on online classification algorithms [18].

Generally, the ELM model is well-suited for human locomotion recognition in amputees due to its reliable performance and simple computational approach. The accuracy of the ELM classifier improves with an increase in the number of neurons in the hidden layer. However, this leads to a higher storage burden due to the large number of parameters, which is detrimental to the real-time forecast on a powered knee prosthesis. To address this limitation, we proposed an improved ELM algorithm that achieves higher accuracy through a smaller number of hidden layer nodes by combining the advantages of the logistic regression (LR) algorithm [19], [20], the hybrid grey wolf optimization and slime mould algorithm (GWO-SMA).

This study aims to develop a real-time intent-recognition system for transfemoral amputees. The system will be capable of accurately recognizing the majority of daily locomotion modes using an improved ELM algorithm. The rest of this paper is organized as follows: Section II introduces the theoretical model of the GWO-SMA algorithm and the improved ELM method. Subsequently, we present a real-time intent-recognition model based on the improved ELM algorithm. Section III presents an experimental study and validation of the real-time intent-recognition model using data collected from four patients. Section IV provides a comprehensive discussion of the current study, and finally, Section V concludes the study. The primary contributions of this paper are outlined below.

(1) A human locomotion intent recognition model based on the improved ELM algorithm was developed, which can recognize 9 common modes of daily locomotion using only 234 parameters with an accuracy of 96.75%.

(2) A real-time prediction system was designed to efficiently identify 6 steady-state modes and 10 locomotion transitions in daily scenes with a prediction time of only 2 ms.

II. METHODS

A. GWO-SMA

In 2020, Li et al. [21] proposed a meta-heuristic algorithm called SMA, inspired by the slime mould in nature. The SMA possesses excellent optimization capabilities and requires fewer parameters, however, it is also susceptible to getting trapped in local optima. One approach to enhance meta-heuristic algorithms is through hybridization, which

TABLE I
INITIALIZE PARAMETERS

Parameter	Value
The number of slime mould	$pop = 50$
Iterations	$T = 50$
Dimension	$dim = 9$
Upper-boundary	$ub = 3$
Lower-boundary	$lb = -3$

involves combining two or more unique characteristics to construct a new algorithm [22], [23]. In 2020, Gao et al. hybridized the GWO algorithm [24] with the SMA [21] and evaluated its performance using three benchmark functions [22]. In this paper, we proposed a GWO-SMA algorithm, which differs from the approach described in reference [22]. The steps of the GWO-SMA algorithm are outlined below.

① the slime mould population is initialized, and the parameter values are set as listed in Table I. The initial positions of the slime moulds are expressed in Eq. (1).

$$X_i = rand \times (ub - lb) + lb \tag{1}$$

where X_i is the position of the i th slime mould, $i \in [1, \ pop]$, ub and lb are the upper and lower boundaries of the search space, respectively. $rand$ is a random number in [0, 1].

② the weight of slime mould, W is updated by Eq. (2).

$$W(SortIndex(i))$$
$$= \begin{cases} 1 + r_1 \times abs\left(\dfrac{S(i) - wF}{aveF - wF}\right), & , i \le 3 \\ 1 + r_2 \times \log\left(\dfrac{bF - S(i)}{bF - wF} + 1\right), & 3 < i \le \dfrac{pop}{2} \\ 1 - r_2 \times \log\left(\dfrac{bF - S(i)}{bF - wF} + 1\right), & \dfrac{pop}{2} < i \le pop \end{cases} \tag{2}$$

$$aveF = \frac{bF + sbF + tbF}{3} \tag{3}$$

where $S(i)$ represents the fitness of X_i, bF and wF are the optimal and worst fitness values obtained in the current iteration, respectively. sbF and tbF are the second-best fitness and the third-best fitness values obtained in the current iteration. r_1 and r_2 are random numbers, which are within the ranges of [0.3, 0.5] and [0, 1] respectively; $aveF$ represents the average value of the bF, sbF, and tbF. The function, $SortIndex$ is defined as follows.

$$SortIndex = sort(S) \tag{4}$$

The top three fitness ranks are given greater emphasis to highlight their importance, while lower weights are assigned to slime mould with lower fitness.

③ the location of the slime mould is updated, the formula of $X(t + 1)$ is as follows:

$$X(t+1) = \begin{cases} r \times (ub - lb) + lb, & , r < z \\ X_b(t) + vb(W \times aveX - X_B(t)), & z \le r < p \\ vc \times X(t), & p \le r \end{cases} \tag{5}$$

$$aveX = \frac{X_b(t) + X_{sb}(t) + X_{tb}(t)}{3} \tag{6}$$

where z denotes the fraction of slime mould individuals randomly distributed within the overall population, the value of z is 0.03 in this paper. r is a random number, which is within the range of [0, 1], and $X_B(t)$ represents an individual randomly selected from slime mould in the t iteration; $X_b(t)$, $X_{sb}(t)$, and $X_{tb}(t)$ are the top three individual locations with the highest odour concentration, and the $aveX$ represents the average value of them; The oscillation parameters, vb and vc are defined as follows.

$$vb = [-a, a] \tag{7}$$

$$vc = [-b, b] \tag{8}$$

Parameters b and a are denoted as follows.

$$b = 1 - \frac{t}{T} \tag{9}$$

$$a = dsigmoid(b) = sigmoid(b) \times (1 - sigmoid(b)) \tag{10}$$

where t and T represent the current iteration and the maximum number of iterations, respectively.

$$p = \tanh(|S(i) - DF|), i = 1, 2, \cdots, N \tag{11}$$

DF denotes the best fitness achieved in all iterations. Through comparing the numerical value of r with z and p to update the position of the $X(t)$.

④ the fitness values are then computed, and the global optimal solution is updated.

⑤ the algorithm terminates if the end condition is satisfied, and proceeds to the second step otherwise. The pseudo-code of the GWO-SMA algorithm is presented in Algorithm 1.

Algorithm 1 Pseudo-Code of the GWO-SMA Algorithm

Inputs: number of slime mould pop, maximum number of iterations T, upper-boundary ub, lower-boundary lb
Output: the best location X_b
1: Initialize: slime mould population $X_i (i = 1, 2, \cdots, pop)$, $t = 0$;
2: While $t < T$ do
3:     Boundary checks were performed on randomly generated slime mould individuals, $X_i \in [lb, ub]$.
4:     Calculate the fitness of all slime mould;
5:     Update best fitness bF, second-best fitness sbF, and third-best fitness tbF;
6:     Update the top three individual locations $X_b(t), X_{sb}(t), X_{tb}(t)$;
7:     Calculate the weight of slime mould W by Eq. (2);
8:     For *each search portion*
9:         Update p, vb, vc;
10:         Update positions by Eq. (5);
11:     End For
12:     $t = t + 1$
13: End While
14: return X_b

The proposed GWO-SMA and SMA algorithms are validated using 12 standard test functions to compare the optimal fitness values and convergence rates achieved by the

Functions	Dim
$f_1(x) = \sum_{i=1}^{n} x_i^2$	9
$f_2(x) = \sum_{i=1}^{n} |x_i| + \prod_{i=1}^{n} |x_i|$	9
$f_3(x) = \sum_{i=1}^{n} \left(\sum_{j-1}^{i} x_j \right)^2$	9
$f_4(x) = \max_i \{ |x_i|, 1 \le i \le n \}$	9
$f_5(x) = \sum_{i=1}^{n-1} \left[100 \left(x_{i+1} - x_i^2 \right)^2 + \left(x_i - 1 \right)^2 \right]$	9
$f_6(x) = \sum_{i=1}^{n} \left([x_i + 0.5] \right)^2$	9
$f_7(x) = \sum_{i=1}^{n} i x_i^4 + random[0, 1]$	9
$f_8(x) = \sum_{i=1}^{n} -x_i \sin\left(\sqrt{|x_i|} \right)$	9
$f_9(x) = \sum_{i=1}^{n} \left[x_i^2 - 10 \cos(2\pi x_i) + 10 \right]$	9
$f_{10}(x) = -20 \exp\left(-0.2 \sqrt{\frac{1}{n} \sum_{i=1}^{n} x_i^2} \right) -$ $\exp\left(\frac{1}{n} \sum_{i=1}^{n} \cos(2\pi x_i) \right) + 20 + e$	9
$f_{11}(x) = \frac{1}{4000} \sum_{i=1}^{n} x_i^2 - \prod_{i=1}^{n} \cos\left(\frac{x_i}{\sqrt{i}} \right) + 1$	9
$f_{12}(x) = \frac{\pi}{n} \{ 10 \sin(\pi y_1) +$ $\sum_{i=1}^{n-1} (y_i - 1)^2 \left[1 + 10 \sin^2(\pi y_{i+1}) \right] + (y_n - 1)^2 \}$ $+ \sum_{i=1}^{n} u(x_i, 10, 100, 4) \quad , y_i = 1 + \frac{x_i + 1}{4}$ $u(x_i, a, k, m) = \begin{cases} k(x_i - a)^m & x_i > a \\ 0 & -a \le x_i \le a \\ k(-x_i - a)^m & x_i < -a \end{cases}$	9

two algorithms. The formulas for the 12 standard test functions are listed in Table II. In this paper, the dimensionality of the functions is equivalent to the number of classifications and the definition domain of the functions belongs to $[-10, 10]$. The qualitative analysis depicted in Fig. 1 illustrates that the proposed GWO-SMA algorithm exhibits a faster convergence rate compared to the SMA across 12 test functions. Moreover, it achieves the optimal fitness value faster and surpasses the original algorithm in terms of attaining the optimal fitness value.

B. Locomotion Intent Recognition Model

The architecture of the human locomotion intent recognition model, which is based on the improved ELM algorithm,
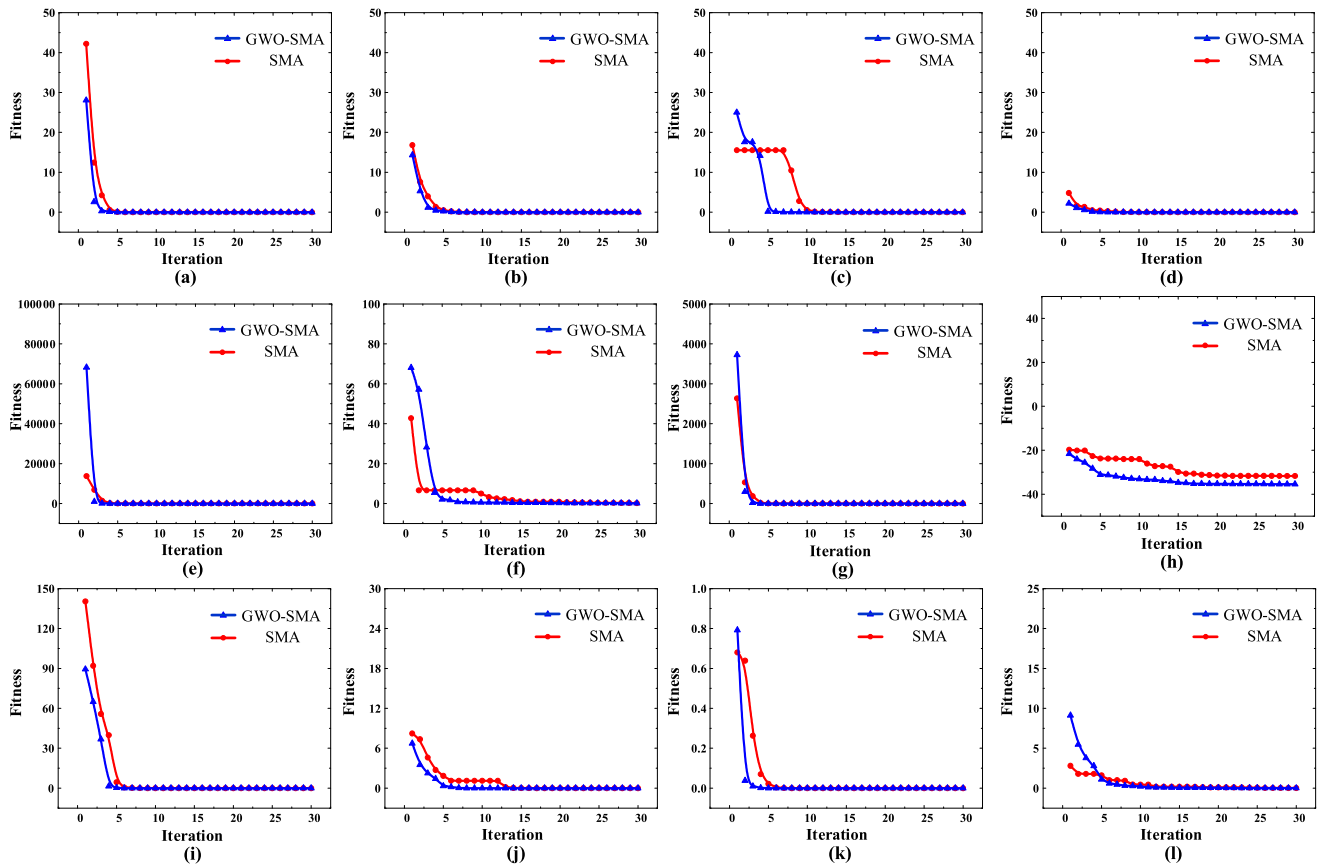
Fig. 1.   Comparisons between GWO-SMA and SMA, (a)-(l) represent the experimental result of the 12 standard test functions, respectively.
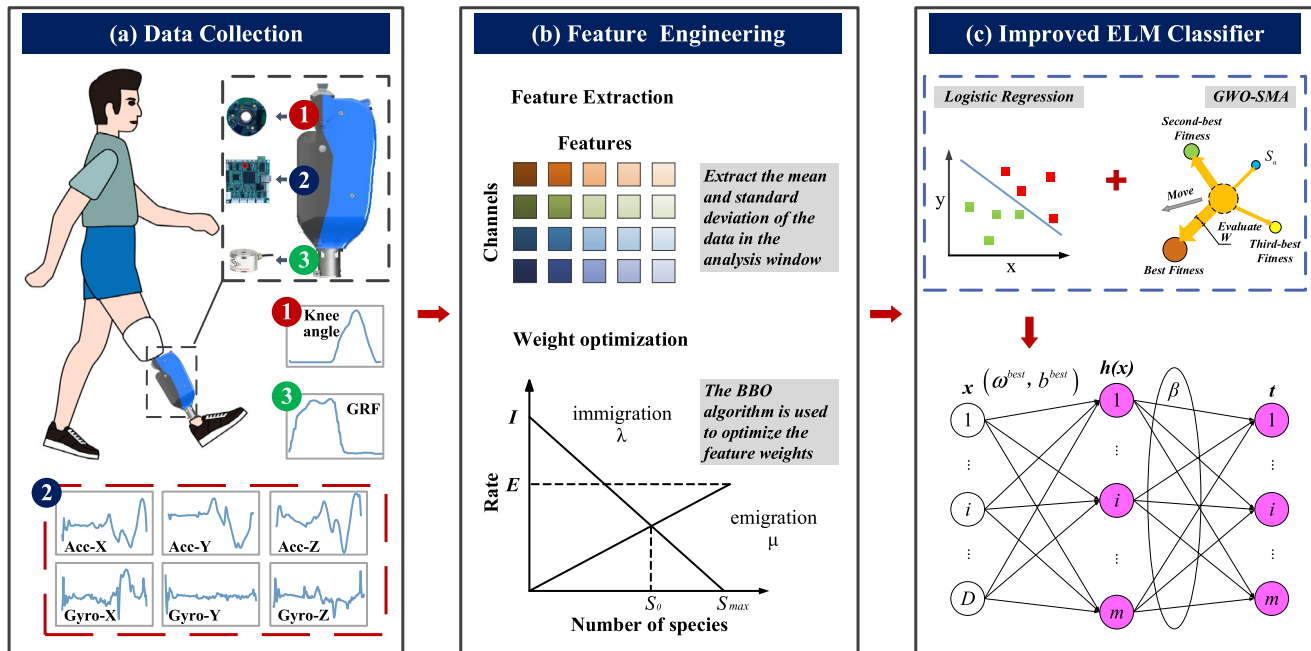

Fig. 2.   Architecture of the human locomotion intent recognition model using an improved ELM classifier, which consists of three parts. (a) The raw data are collected from various sources including a knee joint angle encoder, an axial load cell, and a six-axis IMU, resulting in a total of eight channels of mechanical signals. (b) The feature engineering module consists of two parts: feature extraction and weight optimization. The features are extracted from the raw data and given different weights. (c) The optimized feature vector is fed into the improved ELM classifier for prediction, which is improved by LR classifier and GWO-SMA.

is illustrated in Fig. 2. It consists of three parts: data collection, feature engineering, and an improved ELM classifier.

In Fig. 2 (a), the raw data was collected from a knee joint angle encoder (KingKong® technology, MBS10), an axial

Subject	Sex	Age	Weight (kg)	Height (cm)	Amputation unilateral	Residual limb length (cm)	Amputation reason	Duration (years)
TF01	Male	38	80	174	L	32	Trauma	9
TF02	Male	32	78	165	R	24.5	Trauma	8
TF03	Male	31	64	169	R	26.5	Trauma	13
TF04	Female	52	64	159	L	22.5	Trauma	10

load cell (Fibos®, SBT673), and a six-axis IMU (MPU6050) with a sampling frequency of 100 Hz, encompassing eight channels of mechanical signals from the knee prosthesis. The raw data was then segmented using a analysis window of 200 ms, and fed into the feature engineering module for processing. The feature engineering module includes of two parts: feature extraction and weight optimization. First, features were extracted from the eight-channel raw data in the data matrix. Then, the Biogeography-Based Optimization (BBO) optimizer assigned higher weights to features that are suitable for classification. Finally, the optimized feature vector was fed into the improved ELM classifier for prediction.

The principles and mechanisms of the ELM algorithm are comprehensively described in [13]. Increasing the number of hidden layer nodes in the ELM algorithm enhances its classification effectiveness. However, it also results in a larger parameter set for saving, which negatively impacts real-time prediction on portable devices. In pre-experiment, it was found that the LR algorithm exhibits superior performance in locomotion intent recognition. Nevertheless, due to the limitations in multiclassification scenarios, further improvements are required for this algorithm. Moreover, if the Sigmoid function is used, the artificial neural network without a hidden layer is identical to an LR model [20]. Therefore, the output coefficients and intercepts of the LR algorithm were used to reduce the number of hidden layer nodes in the ELM algorithm, ensuring that the number of hidden layer nodes equals to the number of output layer nodes (classifications, m). Subsequently, the weight vector, ω, consists of the LR output coefficient matrix ω^{LR} and random number matrix rnd^{ω}. To keep the randomness of the ELM algorithm, the GWO-SMA algorithm was adopted for randomly optimizing values $b^{GWO-SMA}$. The bias of the l th hidden node is b_l which is composed of b_l^{LR} and $b_l^{GWO-SMA}$:

$$\omega_l = \omega_l^{LR} + rnd_l^{\omega} \quad l = 1, \ldots, m \quad (12)$$
$$b_l = b_l^{LR} + b_l^{GWO-SMA} \quad l = 1, \ldots, m \quad (13)$$

where $rnd_l^{\omega} \in [-1, 1]$, and $b_l^{GWO-SMA} \in [-2, 2]$. The number of slime moulds is 50, and the number of iterations is 50. The optimal solution is $b^{bGWO-SMA}$. Finally, the optimal weight matrix, ω^{best} and the optimal bias, b^{best} are saved. Fig. 2 (c) displays the model structure of the improved ELM with D input layer nodes, m hidden layer nodes, and m output layer nodes. With the aim of improving the generalization performance of the algorithm, the function of the output

weights β was changed to:

$$\beta = \left(\frac{1}{C} + H^T H \right)^{-1} H^T T \quad (14)$$

where C indicates a weight factor for regularizing the proportion of empirical risk and structural risk. H represents the hidden layer output matrix, and H^T denotes its transposed matrix. T is the target matrix for the training data. The formula for H is given as follows.

$$H(x) = [h_1(x), h_2(x), \cdots, h_m(x)] \quad (15)$$

where, $h_m(x)$ denotes the output of the m th hidden node, the Eq. (16) is expressed as follows.

$$h_m(x) = g\left(\omega_m^{best} x + b_m^{best} \right), \omega_m^{best} \in R^D, b_m^{best} \in R \quad (16)$$

In this paper, we used $Softplus(x)$ as the activation function $g(x)$.

III. EXPERIMENTS AND RESULTS

A. Experimental Protocol

Four subjects (3 males and 1 female) with unilateral TF amputees (TF01—TF04) were recruited, and Table III shows their basic information. The four subjects had various heights (1.59–1.74 m) and weights (64–80 KG). The current study was approved by the Ethics Committee of the Second Hospital of Jilin University (Log#2021072) and was conducted following the guidelines of the Declaration of Helsinki (2013) and the International Ethical Guidelines for Biomedical Research Involving Human Subjects (2002). Before the experiment, each subject underwent more than a week of practice with a powered lower limb prosthesis, ensuring their ability to perform the experiment safely. A certified prosthetist adjusted the parameters based on each subject's height and weight during the control procedure. The speeds and experimental platforms used for nine daily locomotion modes could refer to [25] in detail. The subjects were informed of the purpose and procedures of the experiment before signing an informed consent form. Furthermore, each subject gave their consent for using the identifiable images. As shown in Fig. 3, multi-sensor data was collected sequentially specifically from TF03 for nine locomotion modes.
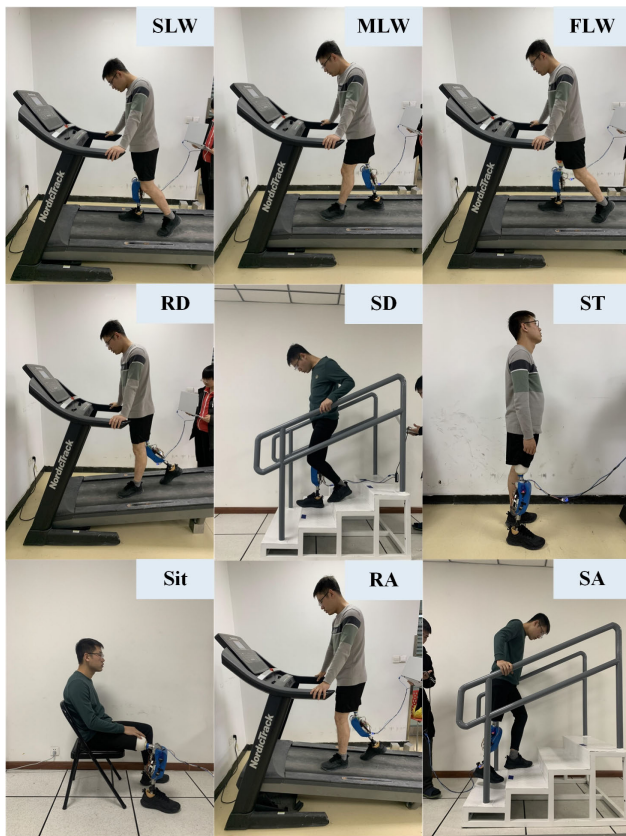
Fig. 3.   Data collection for the nine locomotion modes of TF03.

B. Data Preparation

This study used a powered knee prosthesis for data collection, which was developed by our laboratory team. A comprehensive description of the hardware system design can be found in reference [26]. One of the major advantages of this prosthesis is its ability to automatically adjust the transmission ratio according to the phase in gait. In this paper, a hierarchical control structure was implemented, and an improved ELM classifier, which was extensively discussed in this work, was used to estimate the user's locomotive intention at a high level. Finite state controllers (FSCs) were employed as middle controllers, while an impedance controller served as a low-level controller [25]. The Elmo® motor driver, custom embedded system, and load cell are powered by a 24-V Li-ion battery, with the supply voltage for the joint angle encoder being scaled using a 5-V regulator.

The prosthesis was worn by subjects in nine locomotion modes, and multi-sensor data were collected. Each data group consisted of eight parameters, including knee joint angle, ground reaction force (GRF), three-axis acceleration, and three-axis angular velocity. In addition, a 10-minute rest period was included between each locomotion mode to ensure non-fatigued state during data collection. Features characterizing the data signals were extracted from a 200-ms analysis window before each toe-off event. The mean value and standard deviation of each signal within the analysis window were chosen as mechanical signal features [3], [27], [28], resulting in a feature vector with a size of 16. To assign different weights

	Accuracy rate	Jaccard score	Recall rate	F1 score
ELM	75.68%	61.65%	79.58%	73.61%
LDA	95.46%	91.31%	95.45%	95.43%
LR	95.45%	91.31%	95.52%	95.46%
the proposed model	**96.75%**	**93.71%**	**96.75%**	**96.73%**

to these selected features, the BBO algorithm was employed due to its excellent performance in estimating the optimal solution for the weight assignment. Previous studies have shown that the BBO algorithm is more align with our expectations compared to other optimization algorithms. The BBO algorithm simulates the migration of species between habitats to solve global optimization problems [29]. The weighted mechanical signal feature set was then fed into the improved ELM classifier for training the classification model. The total sample size is 1080, with 120 samples for each locomotion mode consisting of equal amounts of data extracted from four subjects. In this study, the 5-fold cross-validation was used for the training and testing of the classifiers.

C. Recognition Accuracy of the Proposed Model

In the present study, an improved ELM algorithm is put forward for the LR algorithm and ELM algorithm, and its results were compared with those of the LR classifier, ELM classifier, and LDA classifier. The number of hidden nodes in the ELM classifier is equivalent to that of the improved model. Table IV shows the accuracy rate, Jaccard score, recall rate, and F1 score of these four classifiers, which reflect their recognition capabilities.

Fig. 4 (a) shows the confusion matrices of the four classifiers derived from exploring the specific cases of misclassification. The proposed model achieves 96.75% accuracy, which is higher than the other three classifiers. However, the confusion matrix reveals a misclassification among the nine locomotion modes. It was computed and served as an indicator to illustrate the relationship between the target classes and predicted classes. As the confusion matrix shown, it was easy to generate incorrect identifications between (SLW, MLW, FLW) and (MLW, RA, RD). For the ELM classifier, the results indicate significant miscalculations among SLW, MLW, FLW, and SA. In contrast, the proposed model effectively identifies SLW and SA using the same number of hidden layer nodes. However, MLW and SD remained confused with other modes. The receiver operating characteristic (ROC) curve was plotted using the true positive rate as ordinate and the false positive rate as abscissa. The values of AUC (area under the ROC curve) were above 0.9, indicating that the proposed model has high recognition accuracy for all nine daily locomotion modes, which can be found in Fig. 4 (b). Nevertheless, the lowest AUC value of the proposed model occurred at MLW, which is only 0.95, suggesting that the effective classification
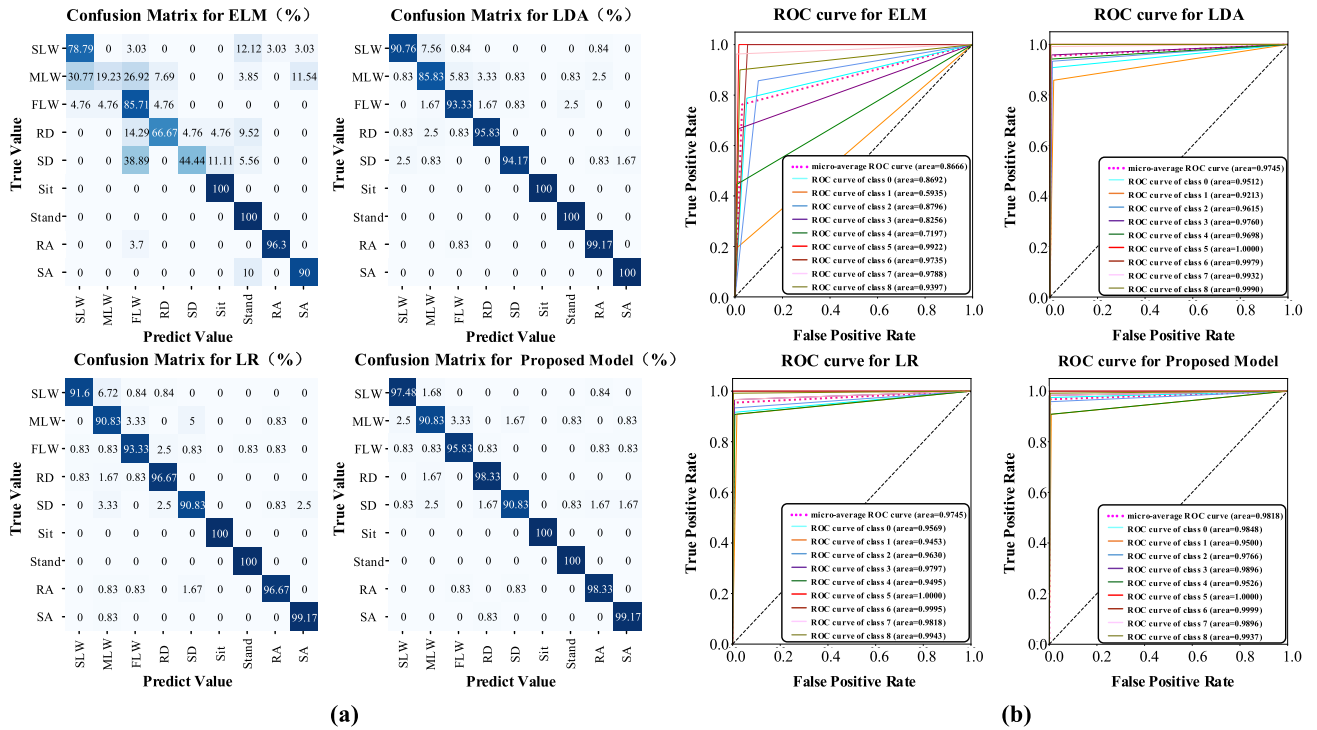
Fig. 4. (a) Confusion matrix for the four classifiers. (b) ROC curve for four classifiers, where classes 0–8 represent SLW, MLW, FLW, RD, SD, Sit, Stand, RA, and SA, respectively.

of level walking at different speeds is still a difficult problem to solve. In this study, only 234 parameters of the improved ELM classifier need to be preserved. The parameters consist of three parts, the optimal input weight matrix, denoted as ω^{best}, the optimal input bias vector, denoted as b^{best}, and the output weight matrix, named as β. The size of ω^{best} is 16×9, which can be defined as the number of features multiplied by the number of classifications. The size of b^{best} is 1×9, which is equal to the number of classifications. The size of β is 9×9, expressed as the number of hidden layer nodes multiplied by the number of classifications. The real-time prediction system based on these parameters has been developed in C by Keil uVision 5 IDE (μVision V5.18.0.0). A 32-bit microchip (STM32F429ZIT6) as the joint controller unit of the knee prosthesis, with a maximum CPU frequency of 180 MHz.

TF03 was again performed under nine locomotion modes within the same experimental environment, and the prediction results and time were recorded. For each locomotion mode, the TF03 walked 30 steps while accurately predicting the number of steps taken. For sitting and standing scenarios, the subject lifted the prosthetic foot off the ground to make a prediction. Out of a total of 270 steps, 258 steps were correctly identified with a prediction time of only 2 ms, which is considerably lower than the required real-time control delay of 300 ms, and the amputee did not perceive the control delay. For real-time human locomotion intent recognition, the prediction processing time, consisted of the time required for extracting the features from the data in the analysis window (B1), formulating and normalizing the feature vector (B2), detecting the gait phase and activating the corresponding classifier (B3), and predicting the user intent (B4) [30]. In this paper, the

middle controller performed phase detection and switching control procedures. Thus, the prediction time of 2 ms was the sum of B1, B2 and B4. The overall computation time was calculated as the difference between two timestamps placed at the start and end points of the intent prediction function.

IV. DISCUSSION

A. Real-Time Locomotion Intention Prediction in a Laboratory Environment

The prediction of human locomotion intentions is a binary classification problem that involves determining whether to maintain the current mode or switch to another mode [31]. To achieve a seamless transition, the improved ELM classifier should use multi-sensor data collected from the prosthesis to predict the upcoming locomotion mode before performing the transition. For real-time experiments on human locomotion intention, TF02 was instructed to walk at a self-selecting medium-speed pace to minimize transitions between locomotion classes. As shown in Fig. 5, this paper investigates ten different locomotion transitions: MLW→SA, SA→MLW, MLW→RD, RD→MLW, MLW→RA, RA→MLW, MLW→SD, SD→MLW, MLW→ST and ST→MLW, respectively. From SA/SD/RA/RD to MLW and vice versa, the transition step starts at the prosthetic side toe-off and ends when the prosthetic heel touches another terrain [11]. Similarly, for MLW→ST and ST→MLW, the transition step begins at the prosthetic side toe-off and ends at the heel-strike on the level ground. We have developed a real-time recognition system based on an offline trained classifier using independent data from TF02 and computed the prediction time of the model.

(a) MLW→SA

(b) SA→MLW

(c) MLW→RD

(d) RD→MLW

(e) MLW→RA

(f) RA→MLW

(g) MLW→SD
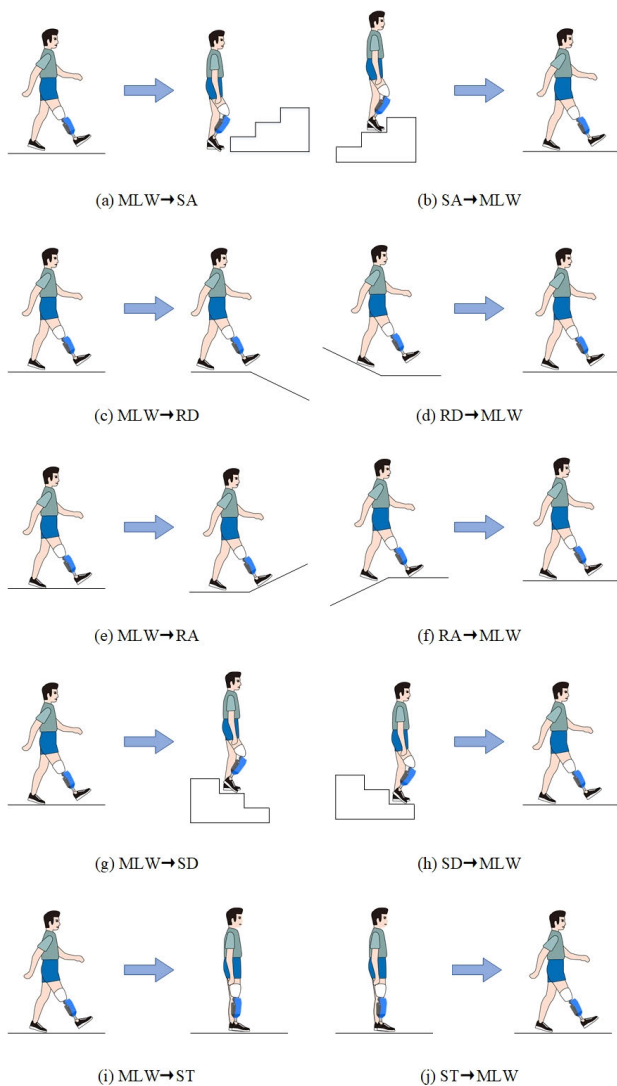
(h) SD→MLW

(i) MLW→ST

(j) ST→MLW

Fig. 5. Schematic diagram of the ten locomotion transitions.

Fig. 6. TF02 performs a real-time intent recognition experiment on a walking/ramp/stairs platform.

TF02 performed a total of 5 trials on the customized platform, with each trail following the circuit: ST→(ST→MLW)→MLW→(MLW→SA)→SA→(SA→MLW)→MLW→(MLW→RD)→RD→(RD→MLW)→MLW→(MLW→RA)→RA→(RA→MLW)→MLW→(MLW→SD)→SD→(SD→MLW)→MLW→(MLW→ST)→ST, as illustrated in Fig. 6. A total of 141 steps were taken by TF02
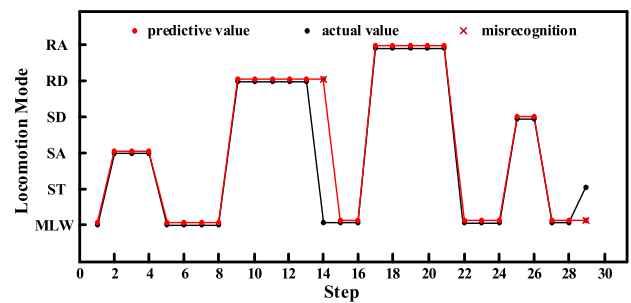

Fig. 7. Comparison between the predictive values and the actual values for a trail.

and the number of correctly predicted steps was recorded. The labels for locomotion transitions are assigned to the upcoming locomotion mode. The predictive values and the actual values for a trail (29 steps) are presented in Fig. 7. Two misrecognitions occurred during this trail, specifically at RD→MLW and MLW→ST. Out of the 141 steps, 133 steps were correctly identified. For trails comprising 141 steps without any classification errors for SD and SA, it was observed that misidentifications between MLW, RA, RD and their respective transitions are prone to occur due to similarities in control procedures within the low-level controller system. It is worth noting that there were some identification errors during the transition from MLW to ST. However, TF02 successfully completed the switch by touching the ground with the prosthesis. Although these incorrect inferences may seem potentially hazardous, they are actually harmless and cannot be noticed by users in these situations. On the other hand, certain misclassifications can be critical as they jeopardize user safety by compromising stability, such as the misidentifying between SA and SD modes.

The comparison between our proposed model and state-of-the-art methods in the field of intent recognition poses challenges due to differences in classifiers, sensors, number of parameters, number of locomotion modes, and accuracy. Since the dataset used in this paper are different from those used in prior studies, only the model structure is compared. As presented in Table V, our model exhibits significantly fewer parameters compared to various state-of-the-art methods and other neural network algorithms. The more complex the model structure, the more parameters need to be saved and the longer the processing time when using the same processor. The authors in references [3], [12], and [32], only trained the classification model offline and evaluated its accuracy without conducting real-time prediction experiments. In reference [25], the authors used the same prosthesis as in this paper to achieve real-time prediction of locomotion intention. However, the model in reference [25] has more parameters that need to be saved and does not seamlessly switch between modes. In our preliminary experiments, we also observed that when the number of model parameters exceeds 500 for a floating-point data type, it consumes excessive memory space, which hinders real-time intention prediction on our prosthesis. Overall, our proposed real-time prediction system efficiently identifies 6 steady-state modes and 10 locomotion transitions with fewer parameters.

TABLE V
COMPARISON WITH STATE-OF-THE-ART METHODS

| Reference	Classifier	Sensors	Number of parameters	Number of locomotion modes	Accuracy (%)
Han et al. 2021 [3]	ABC-IBPNN-DTS	One IMU	>500	9 steady-state modes	96.71
Bruinsma et al. 2021 [12]	RNN	Two IMUs	>500	8 steady-state modes and 24 locomotion transitions	93.06
Feng et al. 2022 [32]	TCCN	A strain gauge and an angle sensor	>500	5 steady-state modes	93.6
Zhang et al. 2023 [25]	The improved KNN	A knee joint angle encoder, an axial load cell, and a six-axis IMU	≥351	9 steady-state modes	96.66
Our Method (steady-state locomotion)	The improved ELM	A knee joint angle encoder, an axial load cell, and a six-axis IMU	234	9 steady-state modes	96.75
Our Method (daily exercise)	The improved ELM	A knee joint angle encoder, an axial load cell, and a six-axis IMU	138	6 steady-state modes and 10 locomotion transitions	94.32
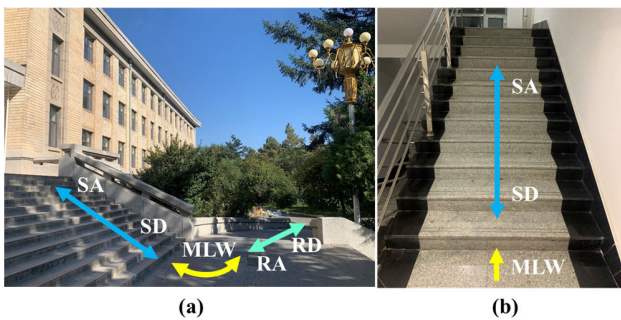
Fig. 8. (a) Outdoor experimental environment and descriptions of various locomotion modes. (b) Indoor corridor environment and descriptions of various locomotion modes.

B. Real-Time Locomotion Intention Prediction in Everyday Scenarios

To validate the proposed predictive model in everyday scenarios, TF02 conducted real-time locomotion experiments in two residential environments, as shown in Fig. 8. During trial 1, TF02 successfully completed six of the most common locomotion modes and ten transitions commonly encountered in daily activities (ST, MLW, SA, SD, RA, RD, ST→MLW, MLW→SA, MLW→SD, MLW→RA, MLW→RD, SA→MLW, SD→MLW, RA→MLW, RD→MLW, MLW→ST). The subject walked a total of 109 steps, which took 89 seconds, close to the speed of a healthy person. The other trial scene was chosen in the corridor, and the TF02 successfully completed three different locomotion modes and four transitions in daily life (MLW, SA, SD, MLW→SA, MLW→SD, SA→MLW, SD→MLW). As a result, the proposed predictive model could be adopted for real-time human locomotion intent recognition on portable devices with a high accuracy. All the detailed experimental videos have been uploaded in the supplementary file.

C. Limitations and Future Works

The main limitation of this paper is the imbalanced distribution of participants in this analysis, with only one female and three males, which may not accurately represent biological sex. We have been continuously recruiting as many subjects as possible to participate in the experiment. However, there are several difficulties in the recruitment process, including psychological factors affecting individual amputees, behavioral limitations specific to amputees, and other factors. In particular, it proves challenging to find female amputees willing to participate in our experiments. This issue is also prevalent among other research groups in the field. In the future, we will recruit more female amputees to validate the proposed model. Another limitation lies in the inability of the proposed predictive model to effectively distinguish between movements at different stair heights and inclinations. To address this concern, we will continue to update the intent recognition model so that it can efficiently identify a wider range of daily locomotion modes and locomotion transitions with sufficient prediction time.

V. CONCLUSION

To conclude, with an aim of reducing the number of parameters in ELM and achieving high accuracy in recognizing nine locomotion modes, we proposed a locomotion intent recognition model based on an improved ELM algorithm. The ELM algorithm was improved using the LR algorithm structure, resulting in a significant reduction in the number of hidden layer nodes. Additionally, the GWO-SMA and BBO algorithms were adopted for finding the optimal solution for the hidden layer bias and optimizing the weight values of each dimension of data, respectively. The proposed model exhibited a significant improvement in accuracy, surpassing both the ELM and LR classifiers. The experimental results showed that the proposed model achieves a recognition accuracy up to 96.75%. Moreover, compared with the ELM classifier, the accuracy of the proposed model was improved by 27.8% when using the same number of hidden layer nodes. However, it is worth noting that classification failures still persist in MLW and SD. Regarding real-time prediction, the processing time for the proposed model was only 2 ms, with only 234 parameters needed to be stored. In addition, two real-life scenarios were conducted to validate the practicality of the proposed model. The study findings provide compelling evidence supporting the feasibility of intent recognition for transfemoral amputees with powered knee prostheses.

REFERENCES

[1] T. Ma et al., "A piecewise monotonic smooth phase variable for speed-adaptation control of powered knee-ankle prostheses," *IEEE Robot. Autom. Lett.*, vol. 7, no. 3, pp. 8526–8533, Jul. 2022.

[2] A. Fleming, W. Liu, and H. Huang, "Neural prosthesis control restores near-normative neuromechanics in standing postural control," *Sci. Robot.*, vol. 8, no. 83, Oct. 2023, Art. no. eadf5758.

[3] Y. Han, C. Liu, L. Yan, and L. Ren, "Design of decision tree structure with improved BPNN nodes for high-accuracy locomotion mode recognition using a single IMU," *Sensors*, vol. 21, no. 2, p. 526, Jan. 2021.

[4] P. Zhang, J. Zhang, and A. Elsabbagh, "Lower limb motion intention recognition based on sEMG fusion features," *IEEE Sensors J.*, vol. 22, no. 7, pp. 7005–7014, Apr. 2022.

[5] X. Chen et al., "A piecewise monotonic gait phase estimation model for controlling a powered transfemoral prosthesis in various locomotion modes," *IEEE Robot. Autom. Lett.*, vol. 7, no. 4, pp. 9549–9556, Oct. 2022.

[6] R. Stolyarov, G. Burnett, and H. Herr, "Translational motion tracking of leg joints for enhanced prediction of walking tasks," *IEEE Trans. Biomed. Eng.*, vol. 65, no. 4, pp. 763–769, Apr. 2018.

[7] Z. Liu, W. Lin, Y. Geng, and P. Yang, "Intent pattern recognition of lower-limb motion based on mechanical sensors," *IEEE/CAA J. Autom. Sinica*, vol. 4, no. 4, pp. 651–660, Oct. 2017.

[8] E. Zheng, L. Wang, K. Wei, and Q. Wang, "A noncontact capacitive sensing system for recognizing locomotion modes of transtibial amputees," *IEEE Trans. Biomed. Eng.*, vol. 61, no. 12, pp. 2911–2920, Dec. 2014.

[9] D. Xu, Y. Feng, J. Mai, and Q. Wang, "Real-time on-board recognition of continuous locomotion modes for amputees with robotic transtibial prostheses," *IEEE Trans. Neural Syst. Rehabil. Eng.*, vol. 26, no. 10, pp. 2015–2025, Oct. 2018.

[10] R. B. Woodward, J. A. Spanias, and L. J. Hargrove, "User intent prediction with a scaled conjugate gradient trained artificial neural network for lower limb amputees using a powered prosthesis," in *Proc. 38th Annu. Int. Conf. IEEE Eng. Med. Biol. Soc. (EMBC)*, Aug. 2016, pp. 6405–6408.

[11] B.-Y. Su, J. Wang, S.-Q. Liu, M. Sheng, J. Jiang, and K. Xiang, "A CNN-based method for intent recognition using inertial measurement units and intelligent lower limb prosthesis," *IEEE Trans. Neural Syst. Rehabil. Eng.*, vol. 27, no. 5, pp. 1032–1042, May 2019.

[12] J. Bruinsma and R. Carloni, "IMU-based deep neural networks: Prediction of locomotor and transition intentions of an osseointegrated transfemoral amputee," *IEEE Trans. Neural Syst. Rehabil. Eng.*, vol. 29, pp. 1079–1088, 2021.

[13] G.-B. Huang, H. Zhou, X. Ding, and R. Zhang, "Extreme learning machine for regression and multiclass classification," *IEEE Trans. Syst. Man, Cybern. B, Cybern.*, vol. 42, no. 2, pp. 513–529, Apr. 2012.

[14] G.-B. Huang, L. Chen, and C.-K. Siew, "Universal approximation using incremental constructive feedforward networks with random hidden nodes," *IEEE Trans. Neural Netw.*, vol. 17, no. 4, pp. 879–892, Jul. 2006.

[15] H.-J. Rong, Y.-S. Ong, A.-H. Tan, and Z. Zhu, "A fast pruned-extreme learning machine for classification problem," *Neurocomputing*, vol. 72, nos. 1–3, pp. 359–366, Dec. 2008.

[16] J. Cao, Z. Lin, G.-B. Huang, and N. Liu, "Voting based extreme learning machine," *Inf. Sci.*, vol. 185, no. 1, pp. 66–77, Feb. 2012.

[17] E. Cambria et al., "Extreme learning machines [trends & controversies]," *IEEE Intell. Syst.*, vol. 28, no. 6, pp. 30–59, Nov. 2013.

[18] S. Ding, N. Zhang, X. Xu, L. Guo, and J. Zhang, "Deep extreme learning machine and its application in EEG classification," *Math. Problems Eng.*, vol. 2015, pp. 1–11, Jan. 2015.

[19] D. Sun, J. Xu, H. Wen, and D. Wang, "Assessment of landslide susceptibility mapping based on Bayesian hyperparameter optimization: A comparison between logistic regression and random forest," *Eng. Geol.*, vol. 281, Feb. 2021, Art. no. 105972.

[20] K. Shah, H. Patel, D. Sanghvi, and M. Shah, "A comparative analysis of logistic regression, random forest and KNN models for the text classification," *Augmented Hum. Res.*, vol. 5, no. 1, p. 12, Mar. 2020.

[21] S. Li, H. Chen, M. Wang, A. A. Heidari, and S. Mirjalili, "Slime mould algorithm: A new method for stochastic optimization," *Future Gener. Comput. Syst.*, vol. 111, pp. 300–323, Oct. 2020.

[22] Z.-M. Gao, J. Zhao, Y. Yang, and X.-J. Tian, "The hybrid grey wolf optimization-slime mould algorithm," *J. Phys., Conf. Ser.*, vol. 1617, no. 1, Aug. 2020, Art. no. 012034.

[23] X. Cheng, J. Li, C. Zheng, J. Zhang, and M. Zhao, "An improved PSO-GWO algorithm with chaos and adaptive inertial weight for robot path planning," *Frontiers Neurorobotics*, vol. 15, Nov. 2021, Art. no. 770361.

[24] Q. Al-Tashi, H. Rais, and S. Jadid, "Feature selection method based on grey wolf optimization for coronary artery disease classification," in *Recent Trends in Data Science and Soft Computing: Proceedings of the 3rd International Conference of Reliable Information and Communication Technology (IRICT 2018)*. Cham, Switzerland: Springer, 2019, pp. 257–266.

[25] Y. Zhang et al., "An optimization system for intent recognition based on an improved KNN algorithm with minimal feature set for powered knee prosthesis," *J. Bionic Eng.*, vol. 20, no. 6, pp. 2619–2632, Nov. 2023.

[26] X. Wang et al., "Design and validation of a polycentric hybrid knee prosthesis with electromagnet-controlled mode transition," *IEEE Robot. Autom. Lett.*, vol. 7, no. 4, pp. 10502–10509, Oct. 2022.

[27] A. J. Young and L. J. Hargrove, "A classification method for user-independent intent recognition for transfemoral amputees using powered lower limb prostheses," *IEEE Trans. Neural Syst. Rehabil. Eng.*, vol. 24, no. 2, pp. 217–225, Feb. 2016.

[28] A. M. Simon et al., "Delaying ambulation mode transition decisions improves accuracy of a flexible control system for powered knee-ankle prosthesis," *IEEE Trans. Neural Syst. Rehabil. Eng.*, vol. 25, no. 8, pp. 1164–1171, Aug. 2017.

[29] F. Liu and G. Xie, "A fast algorithm for community detection of network systems in smart city," *IEEE Access*, vol. 7, pp. 51856–51865, 2019.

[30] F. Zhang and H. Huang, "Source selection for real-time user intent recognition toward volitional control of artificial legs," *IEEE J. Biomed. Health Informat.*, vol. 17, no. 5, pp. 907–914, Sep. 2013.

[31] K. Zhang et al., "Foot placement prediction for assistive walking by fusing sequential 3D gaze and environmental context," *IEEE Robot. Autom. Lett.*, vol. 6, no. 2, pp. 2509–2516, Apr. 2021.

[32] Y. Feng, D. Xue, L. Ju, W. Zhang, and X. Ding, "Small-data-driven temporal convolutional capsule network for locomotion mode recognition of robotic prostheses," *IEEE Trans. Neural Syst. Rehabil. Eng.*, vol. 30, pp. 2540–2548, 2022.